

Article

Origin, Migration, and Accumulation of Crude Oils in the Chaoyang Step-Fault Zone, Fushan Depression, Beibuwan Basin: Insight from Geochemical Evidence and Basin Modeling

Yang Shi ^{1,*}, Hao Guo ¹, Xiaohan Li ¹, Huiqi Li ¹, Meijun Li ^{2,3}, Xin Wang ^{2,*}, Surui Dong ² and Xi He ²

¹ Southern Oil Exploration and Development Company, PetroChina, Haikou 570216, China; guohao1118@cnpc.com.cn (H.G.); lixiaohan01@cnpc.com.cn (X.L.); lihuiqi@cnpc.com.cn (H.L.)

² State Key Laboratory of Petroleum Resources and Engineering, China University of Petroleum (Beijing), Beijing 102249, China; meijunli@cup.edu.cn (M.L.); 2022210087@student.cup.edu.cn (S.D.); 2022215031@student.cup.edu.cn (X.H.)

³ Faculty of Petroleum, China University of Petroleum (Beijing) at Karamay, Karamay 834000, China

* Correspondence: shiy02@cnpc.com.cn (Y.S.); wangxin2021@student.cup.edu.cn (X.W.)

Abstract: The Fushan Depression is a hydrocarbon-rich depression in the Beibuwan Basin, South China Sea. In this study, 14 source rocks and 19 crude oils from the Chaoyang Step-Fault Zone and Southern Slope Zone were geochemically analyzed to determine their origins. The hydrocarbon generation, migration, and accumulation processes were also determined using two-dimensional basin modeling. Crude oils from the low-step area show a close relationship with the source rocks of the first and second members of the Eocene Liushagang Formation (El_{s1} and El_{s2}). The oils from the middle-step area and the Southern Slope Zone are derived from the local source rocks in those areas, in the third member of the Eocene Liushagang Formation (El_{s3}). Hydrocarbons generated from the El_{s3} source rocks of the Southern Slope Zone migrated along sand bodies to the El_{s3} reservoir. The fault system of the Chaoyang Step-Fault Zone controls hydrocarbon migration and accumulation in the low-step and middle-step areas. The resource potential of the middle-step area is limited by its shallow burial depth. The low-step area is a more favorable exploration area due to its proximity to the source kitchen.

Keywords: Fushan Depression; oil source correlation; hydrocarbon migration and accumulation; basin modeling



Citation: Shi, Y.; Guo, H.; Li, X.; Li, H.; Li, M.; Wang, X.; Dong, S.; He, X. Origin, Migration, and Accumulation of Crude Oils in the Chaoyang Step-Fault Zone, Fushan Depression, Beibuwan Basin: Insight from Geochemical Evidence and Basin Modeling. *Energies* **2024**, *17*, 5842. <https://doi.org/10.3390/en17235842>

Academic Editors: Krzysztof Skrzypkowski and Reza Rezaee

Received: 19 October 2024
Revised: 11 November 2024
Accepted: 20 November 2024
Published: 21 November 2024



Copyright: © 2024 by the authors. Licensee MDPI, Basel, Switzerland. This article is an open access article distributed under the terms and conditions of the Creative Commons Attribution (CC BY) license (<https://creativecommons.org/licenses/by/4.0/>).

1. Introduction

Understanding the oil–source relationships and hydrocarbon accumulation process is crucial for determining favorable exploration targets [1–3]. The Fushan Depression is an important hydrocarbon-rich depression in the Beibuwan Basin, South China Sea, with an area of 29,200 km². The oils discovered in the region originate from the source rocks of the Paleogene Liushagang Formation (El_{s}) [4,5]. Two secondary faults—the Meihua and Lianhua Faults—divide the entire Fushan Depression into the Huangtong/Bailian Sag and the Southern Slope Zone. The tectonic transfer zone in the central part of the depression is related to the regional tectonic stress field [6–8]. In the early stages of exploration, the main hydrocarbon target areas were the tectonic transfer zone and the eastern part of the Southern Slope Zone. The depositional characteristics, tectonic style, and hydrocarbon accumulation model of this area have been described in detail [9–13]. In recent years, the western area of the Fushan Depression has shown great exploration potential, with the discovery of the Chaoyang, Yong’an, Hongguang, and Meitai oilfields [4,14].

Geochemical analysis has identified three oil groups in the area [14,15], and all the Paleogene reservoirs in the depression were charged in the same, single hydrocarbon charging episode [14,16]. The effective source rocks in the western area of the Fushan

Depression are in the central and northern parts of the Huangtong Sag, and the Chaoyang and Yong'an areas adjacent to the Huangtong Sag are expected to be favorable exploration areas [4]. The Chaoyang Step-Fault Zone, located in the northwest margin of the Fushan Depression, is divided into middle- and low-step areas by the Bohou Fault. The low-step area is adjacent to the Huangtong Sag and has attracted increasing attention for its exploration potential [17]. However, hydrocarbons have also been discovered in the middle-step area in recent years, although their geochemical characteristics and origins have not been confirmed and the correlation between the oils in the middle-step and the low-step areas has not yet been established. Against this background, systematic analysis of the origins, migration, and accumulation of the hydrocarbons in the Chaoyang Step-Fault Zone is essential to understanding the exploration potential of the area.

In this study, oil sources were identified by geochemical analysis. The hydrocarbon migration and accumulation processes were determined using basin modeling techniques, supported by fluid inclusion data. A comprehensive understanding of the origins and accumulation of hydrocarbons in the study area is of great significance for determining favorable exploration areas and reducing oil and gas exploration risk.

2. Geological Setting

The Fushan Depression, located in the southeast of the Beibuwan Basin, is a typical rift subsidence lacustrine basin characterized by multiphase structural superposition. The western area of the depression is divided into the Chaoyang Step-Fault Zone, the Huangtong Sag, and the Southern Slope Zone from north to south (Figure 1). In the Chaoyang Step-Fault Zone, two areas—the middle-step area and the low-step area—are divided by the Bohou Fault.

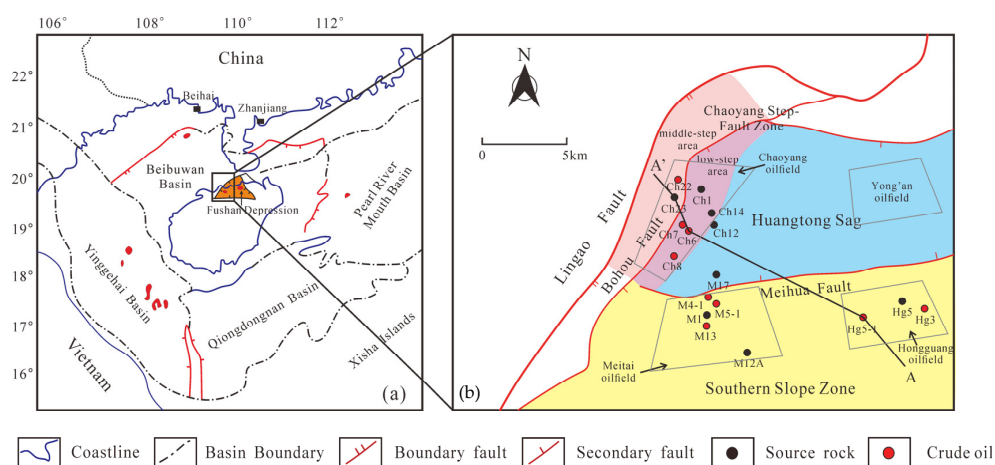


Figure 1. Geological maps showing (a) the location of the Fushan Depression and (b) the tectonic distribution units and sampling wells in the Fushan Depression.

The Shenhu, Zhuqiong, and Nanhai tectonic movements, which occurred in the Paleogene, controlled the deposition of the Changliu Formation (*Ech*), the Liushagang Formation (*Els*), and the Weizhou Formation (*Ewz*), respectively [8]. The Changliu Formation and Weizhou Formation are mostly conglomerate-bearing sandstone and sandy mudstone deposits (the sedimentary facies is shown in the Figure 2) [18]. The Liushagang Formation is generally a delta-lacustrine sedimentary system, and is the main source and oil-bearing bed. Small amounts of hydrocarbon accumulated in the Changliu Formation and Weizhou Formation. The Liushagang Formation is divided into three sub-members—*Els*₃, *Els*₂, and *Els*₁, corresponding to the *SQl*₃, *SQl*₂, and *SQl*₁ sequences, respectively (Figure 2) [18]. The sediments were supplied from the fan delta in the northwestern margin and the braided river delta in the southern margin [19–21]. The *Els*₃ stratum is missing in the low-step area and the Huangtong Sag, which may be due to the extension of the Bohou and Meihua Faults (Figure 1).

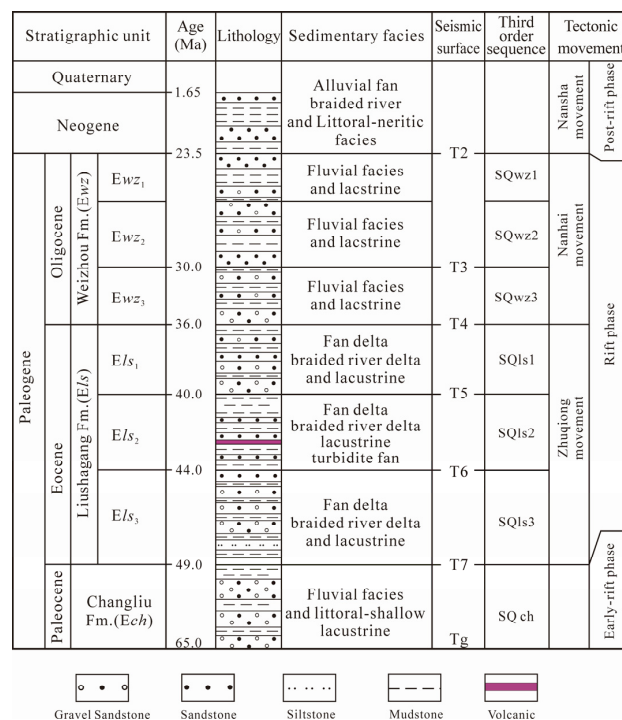


Figure 2. Stratigraphic column and sequence division of the Fushan Depression (After Ma et al., 2012 [12]).

The crude oils found in the Southern Slope Zone are mainly in Els_3 , whereas the reservoirs in the low-step area of the Chaoyang Step-Fault Zone are in Els_1 and Els_2 . In recent years, hydrocarbon shows have also been discovered in the Els_3 and Ech in the middle-step area.

3. Samples and Methods

3.1. Samples

A total of 51 source rock samples were collected from the Chaoyang Step-Fault Zone and the Southern Slope Zone, including Els_3 source rocks from the middle-step area, Els_1 and Els_2 source rocks from the low-step area, and Els_3 source rocks from the Southern Slope Zone. The sampling wells are shown in Figure 1. Total organic carbon (TOC) content measurement and pyrolysis analysis were performed to identify their hydrocarbon generation potential. Fourteen samples were selected for further biomarker analysis. Nine crude oils were collected from the Chaoyang Step-Fault Zone; seven from the Els_1 and Els_2 reservoirs in the low-step area; and two from the Els_3 and Ech reservoirs in the middle-step area. In addition, ten sets of geochemical data were collected from previous studies to compare the distinctions of crude oils between the Southern Slope Zone and the Chaoyang Step-Fault Zone [14]. Oil-source correlation was carried out for the core and oil samples using gas chromatography–mass spectrometry (GC–MS) on the saturated and aromatic fractions. In addition, two Ech reservoir sandstone samples from Well Ch23, drilled in the middle-step area, were polished for fluid inclusion observation and homogenization temperature measurement.

3.2. Geochemical Experiment

The core sample was ground into powder of less than 80 mesh. Carbonates were removed from the rock samples with hydrochloric acid prior to TOC measurement using a LECO CS-230 carbon sulfur analyzer manufactured by LECO in American (St. Joseph, MI, USA). The rock-eval parameters were obtained by heating 100 mg samples to 600 °C using an OGE-VI-type pyrolyzer manufactured by Institute of Petroleum Exploration & Development in China (Beijing, China). The rock powder was extracted for 24 h using a

Soxhlet apparatus with 400 mL of dichloromethane and methanol as the solvent (93:7, v:v). Asphaltene was removed from the source rock extracts and crude oil samples with 50 mL of n-hexane. The residue was separated into saturated and aromatics hydrocarbons in an alumina/silica gel column using 30 mL n-hexane and dichloromethane: n-hexane (2:1, v:v), respectively, as eluents. The biomarker compositions of the saturated and aromatic fractions were obtained using an Agilent 6890 GC–Agilent 5975i mass spectrometry system and an Agilent 7890B GC–Agilent 5977A MS system, respectively. The instruments were made by Agilent Corporation in American (Santa Clara, CA, USA).

Fluid inclusions were observed using a Leica polarization fluorescence microscope and fluorescence photometer, which were made in China. The homogenization temperatures were measured on brine inclusions associated with the hydrocarbons using the heating–freezing stage of a Linkham Model THMSG 600, which manufactured by Linkham Corporation in UK (Salfords, UK). The temperature was raised from 24 °C (room temperature) to the homogeneous temperature (Th) at a rate of 5 °C/min, and then held at Th for 1 min for temperature measurement.

3.3. Basin Modeling

Basin modeling is an effective tool for the analysis of hydrocarbon generation, migration, and accumulation [22]. A representative profile was selected for 2D basin modeling, and the process was as follows: (1) Stratigraphic model and fault model construction. The geological data, including stratigraphic data, fault data, well data, and erosion thickness, were collected from the Southern Oil Exploration and Development Company. The sealing capability of faults was assigned based on the main active periods. (2) Lithofacies model construction. The models were constructed according to the lithology and sedimentary characteristics of representative wells (Figure 3). The Liushagang Formation contains three lithofacies—deltaic mudstone, lacustrine mudstone, and sandstone. The deltaic and lacustrine mudstone serve as the source rocks. The TOC content and hydrocarbon index (HI) values for the source rocks were averaged from the experimental data. The Burnham (1989) T-II kinetics model was applied for hydrocarbon generation simulation [23], and the EASY% Ro model was applied for maturity calculation [24]. (3) Boundary condition setting. The paleo-water depths (PWD) for different positions and stratigraphic units were assigned based on their sedimentary facies [25]. The paleo-heat flow (PHF) was determined based on previous literature [14,26,27], and the sediment–water interface temperatures (SWIT) were obtained from the global paleothermal database [28]. Finally, a hybrid algorithm combining Darcy and percolation was used for hydrocarbon migration simulation.

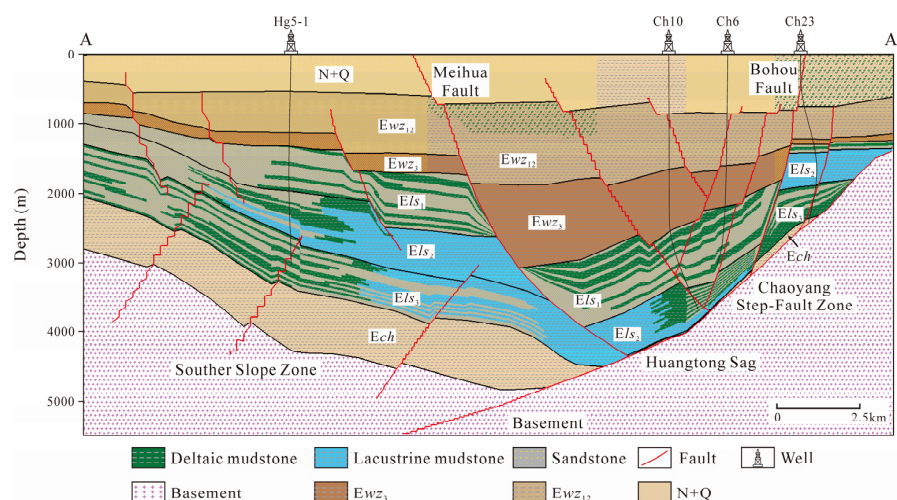


Figure 3. Two-dimensional lithofacies models for the representative profiles in the Chaoyang Step-Fault Zone.

4. Results and Discussion

4.1. Hydrocarbon Generating Potential of Source Rocks

Gray-dark mudstones occur widely in the study area, with TOC contents varying from 1.02% to 2.50%, and an average of 1.50%. The hydrocarbon potential index (S_1+S_2) is in the range of 1.71~10.06 mg/g. The S_1+S_2 versus TOC plot indicates good–excellent source rocks (Figure 4a, Table 1). The hydrogen index (HI) ranges from 136 to 414 mg/g, with the HI versus Tmax plot indicating the type II₁ and II₂ kerogen (Figure 4b, Table 1). There are no evident differences in hydrocarbon generation potential and kerogen types among the El_{s1} , El_{s2} , and El_{s3} source rocks. The El_{s3} source rocks from the Southern Slope Zone have slightly higher Tmax values, suggesting their relatively higher maturity.

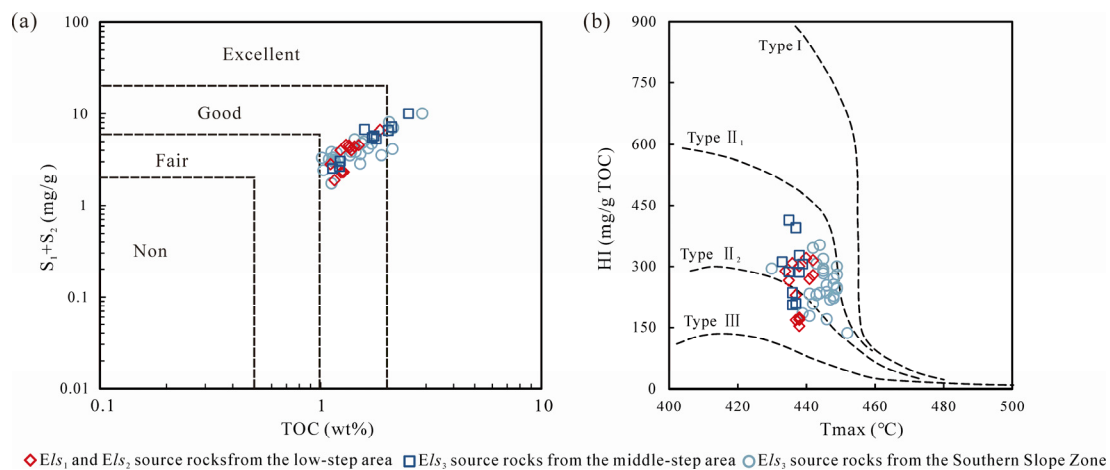


Figure 4. Variation of (a) (S_1+S_2) with total organic carbon (TOC) content and (b) hydrogen index with Tmax for source rocks from the Fushan Depression showing the hydrocarbon-generating potential and organic matter type, respectively. (modified after Robison et al., 1999 [29] and Mukhopadhyay et al., 1995 [30]).

Table 1. TOC and rock-eval pyrolysis data for the Liushagang Formation source rock samples in the Fushan Depression.

Area	Well	Depth/m	Fm.	TOC	Tmax	S_1	S_2	HI
Middle-step area	Ch23x	2036-2040	El_{s3}	1.74	438	0.08	5.71	328
	Ch23x	2085-2089	El_{s3}	2.50	437	0.17	9.89	396
	Ch23x	2135-2139	El_{s3}	1.58	435	0.21	6.54	414
	Ch23x	2187-2191	El_{s3}	1.22	437	0.08	2.55	209
	Ch23x	2235-2239	El_{s3}	1.71	439	0.31	5.24	306
	Ch23x	2285-2289	El_{s3}	1.78	438	0.26	5.09	285
	Ch23x	2335-2339	El_{s3}	2.02	435	0.82	5.79	286
	Ch23x	2386-2390	El_{s3}	2.10	433	0.69	6.53	311
	Ch23x	2435-2439	El_{s3}	1.23	436	0.14	2.89	236
	Ch23x	2535-2539	El_{s3}	1.13	436	0.18	2.33	206
Low-step area	Ch1	2392.5	El_{s1}	1.16	438	0.08	1.77	153
	Ch1	2467.88	El_{s1}	1.34	436	0.39	4.14	308
	Ch2	2491.5	El_{s1}	1.27	437	0.15	2.14	168
	Ch2	2493.5	El_{s1}	1.24	438	0.11	2.15	174
	Ch2	2622.5	El_{s1}	1.26	438	0.14	2.13	169
	Ch6x	2412.1	El_{s1}	1.11	437	0.24	2.55	230
	Ch6x	2682.5	El_{s1}	1.42	434	0.29	4.1	288
Ch6x	2686.1	El_{s1}	1.36	438	0.18	4.07	300	

Table 1. Cont.

Area	Well	Depth/m	Fm.	TOC	Tmax	S ₁	S ₂	HI
Southern Slope Zone	Ch12x	2545.2	El _{s1}	1.38	435	0.32	3.65	265
	Ch12x	3473.5	El _{s2}	1.86	440	0.68	5.95	321
	Ch12x	3476	El _{s2}	1.30	442	0.47	4.11	315
	Ch12x	3512.2	El _{s2}	1.49	441	0.55	4	269
	Ch12x	3513.6	El _{s2}	1.23	442	0.54	3.42	278
	Hg5	2731	El _{s3}	1.36	448	0.4	3.1	228
	Hg5	2732	El _{s3}	1.51	447	0.3	3.32	219
	Hg5	2733.5	El _{s3}	1.15	448	0.2	2.93	255
	M1	3075.07	El _{s3}	1.54	449	0.46	4.29	279
	M1	3076.66	El _{s3}	2.03	449	0.57	6.1	300
	M1	3108.42	El _{s3}	2.89	445	0.88	9.18	318
	M1	3112.88	El _{s3}	1.12	452	0.19	1.52	136
	M1	3169.48	El _{s3}	1.51	446	0.27	2.57	170
	M2	3004.5	El _{s3}	1.03	442	0.25	2.15	209
	M2	3045	El _{s3}	1.20	443	0.36	2.76	230
	M2	3046.3	El _{s3}	1.14	446	0.42	2.89	253
	M2	3051	El _{s3}	1.43	442	0.35	4.93	346
	M4	3215	El _{s3}	1.44	443	0.51	3.31	230
	M4	3217	El _{s3}	2.05	444	0.86	7.22	353
	M4	3218.5	El _{s3}	1.15	446	0.27	2.71	236
	M4	3221	El _{s3}	1.12	443	0.39	3.44	307
	M4	3222.5	El _{s3}	1.18	445	0.38	3.34	283
	M4	3223.5	El _{s3}	1.57	445	0.47	4.52	289
	M4	3228.5	El _{s3}	1.16	444	0.33	2.71	234
	M12Ax	2660	El _{s3}	2.13	430	0.76	6.27	295
	M17x	3799.2	El _{s3}	1.02	445	0.3	2.99	295
	M17x	3802	El _{s3}	1.09	448	0.23	2.94	269
	M17x	3803.5	El _{s3}	1.38	449	0.41	3.41	248
	M17x	3804.4	El _{s3}	1.70	449	0.53	4.18	245
	M17x	3805	El _{s3}	1.17	448	0.33	2.6	223

Note: TOC: total organic carbon, wt%; Tmax: temperature at maximum generation, °C; S₁: volatile hydrocarbon content, mg HC/g rock; S₂: remaining hydrocarbon generative potential, mg HC/g rock; HI: hydrogen index = S₂*100/TOC, mg HC/g TOC; Fm.: Formation.

4.2. Oil–Oil and Oil–Source Rock Correlations

The crude oils discovered in the middle-step area can be distinguished from that of the low-step area by analysis of the molecular markers in the saturated and aromatic hydrocarbons. Oil–source rock correlation indicates that the middle-step oils may be sourced from the local El_{s3} source rocks.

4.2.1. Normal Alkanes and Acyclic Isoprenoids

The total ion chromatogram (TIC) of the selected oil samples is shown in Figure 5. All the crude oils contain a complete normal alkanes distribution with carbon numbers ranging from nC₁₂ to nC₃₅. No evident odd carbon preference was observed in any of the oil samples, with both the carbon preference index (CPI) and the odd–even predominance (OEP) ratios being lower than 1.20, which suggests mature crude oils. All of the samples show high pristane (Pr) contents relative to phytane (Ph), with the Pr/Ph ratios ranging from 3.36 to 4.45, indicating that the source rocks were deposited in a typical oxidizing environment (Figure 5).

4.2.2. Distribution of Terpanes and Hopanes

Tricyclic terpanes were detected in all the source rock and crude oil samples. The El_{s1} and El_{s2} crude oils have relatively higher contents of C₁₉ TT, C₂₀ TT, and oleanane (OL), with the C₁₉₊₂₀/C₂₁TT and OL/C₃₀H in the ranges 3.43~4.16 and 0.25~0.43, respectively (Figures 6 and 7). The El_{s3} crude oils are characterized by high abundance of C₂₃ TT and

low abundance of oleanane, with $C_{19+20}/C_{21}TT$ and $OL/C_{30}H$ in the ranges 1.66~2.64 and 0.15~0.24, respectively. (Figures 6 and 7). Three unusual tetracyclic terpanes were present in all the crude oil samples, identified as C_{24} -des-A-oleanane, C_{24} -des-A-lupane, and C_{24} -des-A-ursane (marked by peaks Y_1 , X_1 , and Z). The ElS_1 and ElS_2 crude oils and source rocks contain high levels of these unusual tetracyclic terpanes, where the levels in the ElS_3 crude oil and source rocks are low (Figure 6).

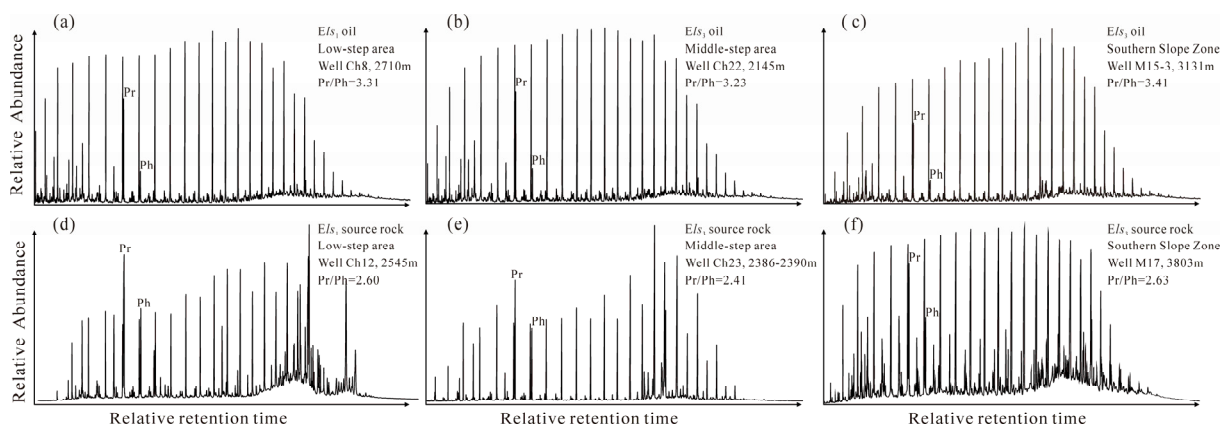


Figure 5. Total ion chromatogram (TIC) of the oil samples and source rocks from the Fushan Depression. (a) ElS_1 oil from low-step area, well Ch8, 2710 m; (b) ElS_3 oil from middle-step area, well Ch22, 2145 m; (c) ElS_3 oil from Southern Slope Zone, well M15-3, 3131; (d) ElS_1 source rock from low-step area, well Ch12, 2545 m; (e) ElS_3 source rock from middle-step area, well Ch23, 2386–2390 m; (f) ElS_3 source rock from Southern Slope Zone, well M17, 3803 m.

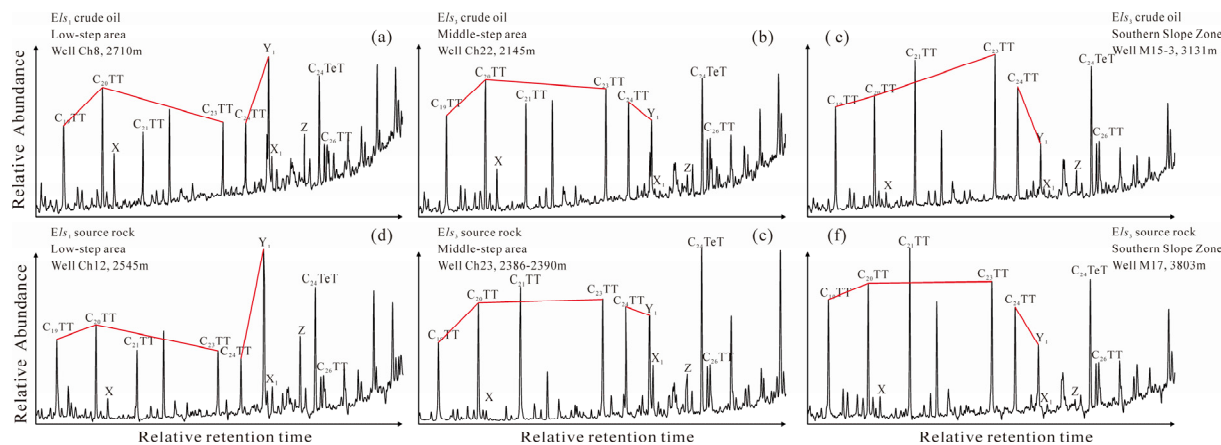


Figure 6. Mass chromatograms (m/z 191) showing the distribution of tricyclic and tetracyclic terpanes in the crude oils and source rocks from the Fushan Depression. (a) ElS_1 oil from low-step area, well Ch8, 2710 m; (b) ElS_3 oil from middle-step area, well Ch22, 2145 m; (c) ElS_3 oil from Southern Slope Zone, well M15-3, 3131; (d) ElS_1 source rock from low-step area, well Ch12, 2545 m; (e) ElS_3 source rock from middle-step area, well Ch23, 2386–2390 m; (f) ElS_3 source rock from Southern Slope Zone, well M17, 3803 m.

C_{19} and C_{20} TT are more abundant in source rocks deposited in shallow-water environments with terrigenous plant input, while $C_{23}TT$ predominates in crude oils from normal marine and saline lacustrine environments. The TT series is less affected by thermal maturity and biodegradation, so their relative contents can be used as effective indicators for oil–oil and oil–source correlation [31,32]. Oleanane (OL) is considered to be derived from angiosperm, which is generally abundant in source rocks and crude oils with high inputs from terrestrial plants. Three unusual tetracyclic terpanes (Y_1 , X_1 , and Z) were

identified, which are similar to oleanane, lupane, and ursane in their molecular structure, and may also originate from higher plants [33–35]. Related parameters, such as $OL/C_{30}H$, $Y_1/(Y_1+C_{24}TT)$, $X_1/(X_1+C_{24}TT)$, and $Z/(Z+C_{24}TT)$, are commonly applied for oil–source correlation [34,36]. The Els_1 , Els_2 , and Els_3 source rocks show significant differences in their organic matter sources. The Els_1 and Els_2 source rocks are rich in $C_{19}TT$, $C_{20}TT$, oleanane, and the unusual tetracyclic terpanes, suggesting a greater contribution from terrestrial plants. The Els_3 source rocks are characterized by a high content of $C_{23}TT$ and low contents of oleanane and the unusual tetracyclic terpanes, indicating predominantly algal input.

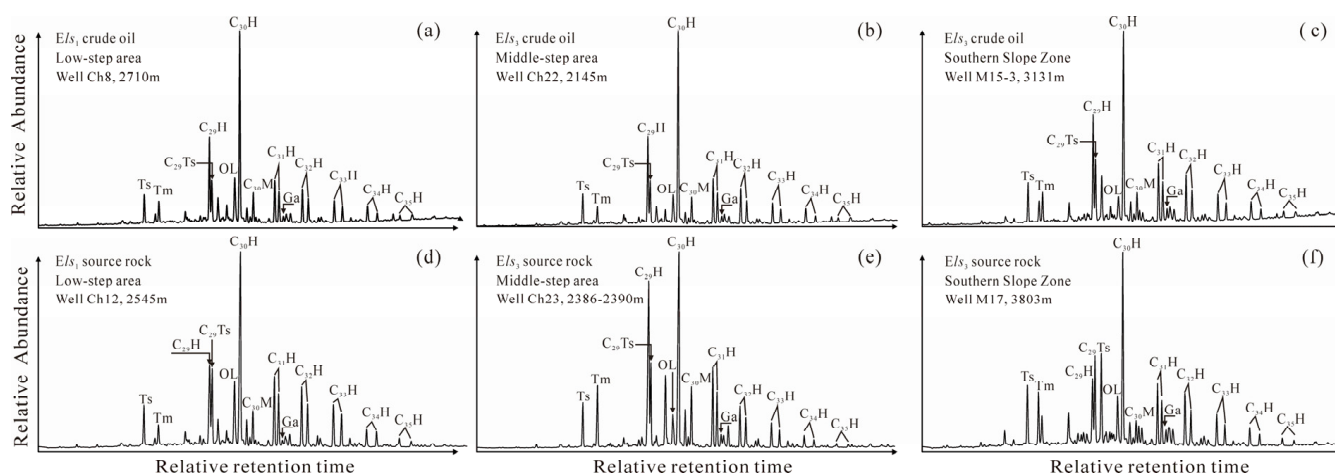


Figure 7. Mass chromatograms (m/z 191) showing the distribution of hopanes in crude oils and source rocks from the Fushan Depression. (a) Els_1 oil from low-step area, well Ch8, 2710 m; (b) Els_3 oil from middle-step area, well Ch22, 2145 m; (c) Els_3 oil from Southern Slope Zone, well M15-3, 3131; (d) Els_1 source rock from low-step area, well Ch12, 2545 m; (e) Els_3 source rock from middle-step area, well Ch23, 2386–2390 m; (f) Els_3 source rock from Southern Slope Zone, well M17, 3803 m.

The distinguishing factors between the oil samples and the correlations between oil and source rocks are shown in Figure 8. The results suggest that the crude oils in the Chaoyang Step Zone are divided into two groups: an oil family distributed in the low-step area and outlier oils derived from the Els_3 source rocks in the middle-step area. The distribution of terpanes in these outlier oils is consistent with the Els_3 crude oils from the Southern Slope Zone (Figure 8).

4.2.3. Distribution of Steranes and Methyl Triaromatic Steroids

The distribution of C_{27} – C_{29} regular steranes (C_{27} – C_{29} St) in source rocks and crude oils reflects the organic matter input. All the crude oils in the study are characterized by “V-shaped” distribution patterns of C_{27} – C_{28} – C_{29} steranes, indicating mixed contributions from lower aquatic organisms and higher plants in the related source rocks [35]. C_{30} 4 α -methyl-24-ethylcholestanes (C_{30} 4-Me St) and triaromatic dinosteroids (dino-TAS) were also detected in both the source rock and crude oil samples (Figures 9 and 10). The Els_3 source rocks and crude oils from the Southern Slope Zone contain high levels of C_{30} 4-Me St and low levels of dino-TAS, with the triaromatic dinosteroid index (TDSI) varying from 0.22 to 0.32. In contrast, dino-TAS is present in the crude oils and source rocks from the Chaoyang Step-Fault Zone (both the low-step area and the middle-step area) in considerable abundance with higher TDSI, ranging from 0.33 to 0.59, with an average of 0.42.

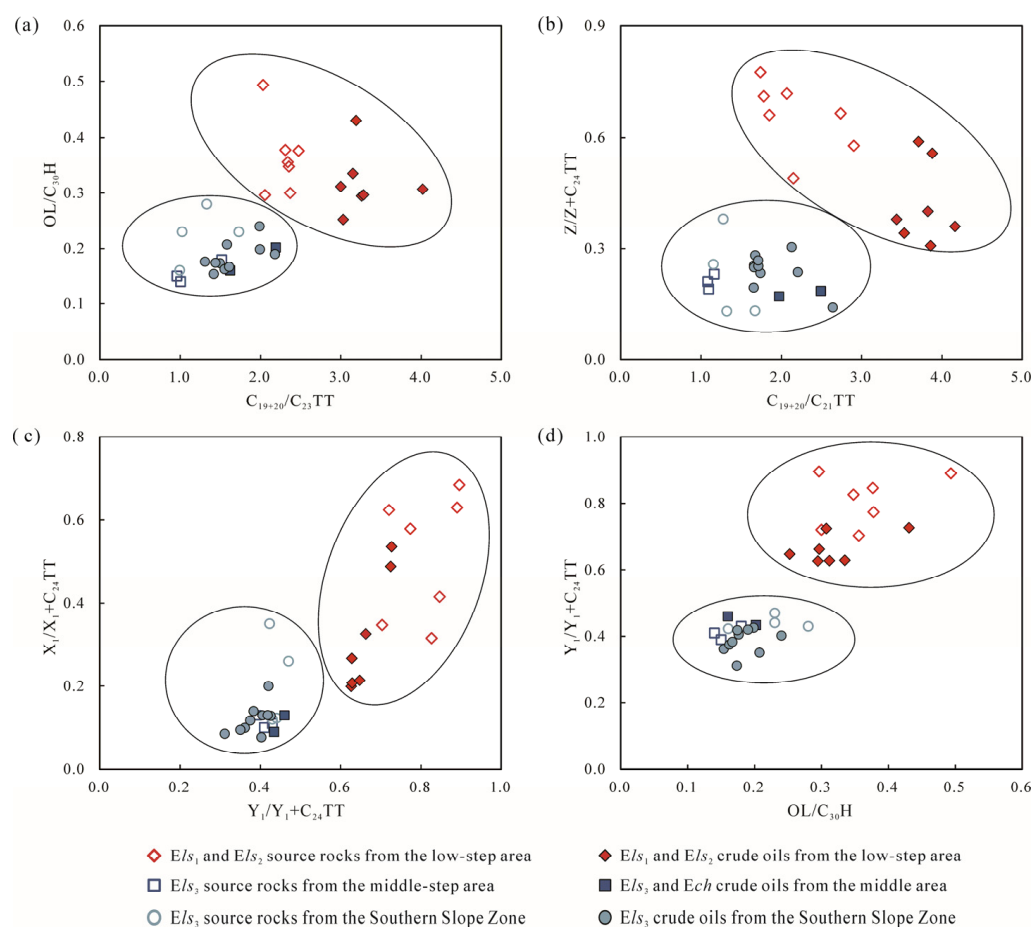


Figure 8. Correlation between the relative abundance of tri- and tetracyclic terpanes in the studied oils and source rocks. (a) $OL/C_{30}H$ vs. $C_{19+20}/C_{23}TT$; (b) $Z/(Z+C_{24}TT)$ vs. $C_{19+20}/C_{21}TT$; (c) $X_1/(X_1+C_{24}TT)$ vs. $Y_1/(Y_1+C_{24}TT)$; (d) $Y_1/(Y_1+C_{24}TT)$ vs. $OL/C_{30}H$. Note: OL = oleanane; TT = tricyclic terpene; $Y_1 = C_{24}$ -des-A-oleanane, $X_1 = C_{24}$ -des-A-lupane, $Z = C_{24}$ -des-A-ursane.

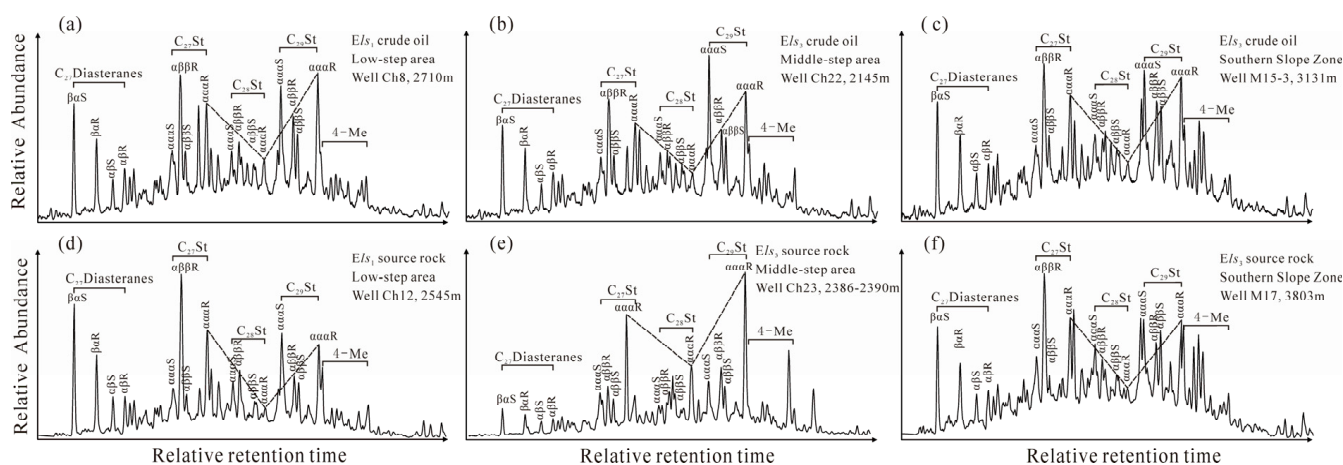


Figure 9. Mass chromatograms (m/z 217) showing the distributions of steranes in crude oils and source rocks from the Fushan Depression. (a) Els_1 oil from low-step area, well Ch8, 2710 m; (b) Els_3 oil from middle-step area, well Ch22, 2145 m; (c) Els_3 oil from Southern Slope Zone, well M15-3, 3131 m; (d) Els_1 source rock from low-step area, well Ch12, 2545 m; (e) Els_3 source rock from middle-step area, well Ch23, 2386–2390 m; (f) Els_3 source rock from Southern Slope Zone, well M17, 3803 m.

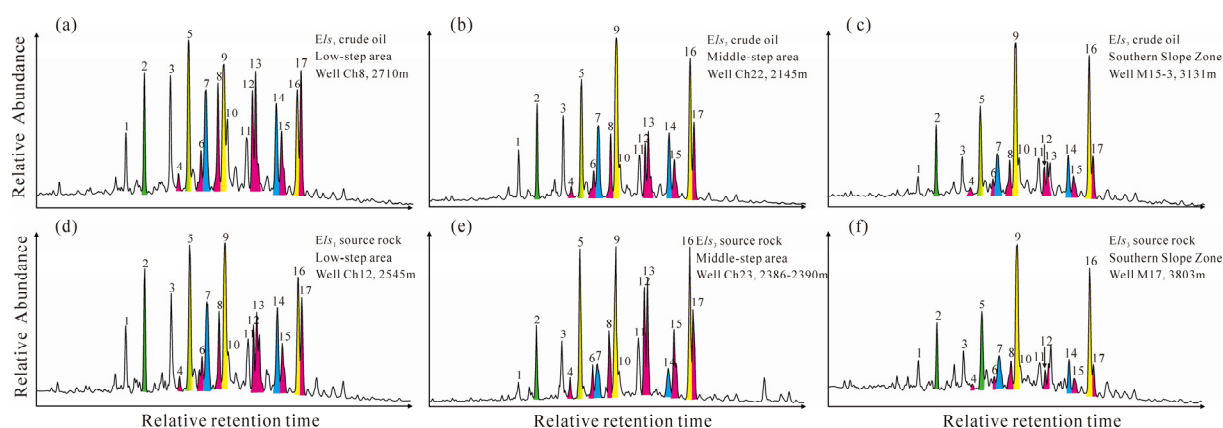


Figure 10. Mass chromatograms (m/z 245) of the aromatic fraction showing the distribution of methyl-triaromatic steroids in crude oils and source rocks from the Fushan Depression. (a) Els_1 oil from low-step area, well Ch8, 2710 m; (b) Els_3 oil from middle-step area, well Ch22, 2145 m; (c) Els_3 oil from Southern Slope Zone, well M15-3, 3131; (d) Els_1 source rock from low-step area, well Ch12, 2545 m; (e) Els_3 source rock from middle-step area, well Ch23, 2386–2390 m; (f) Els_3 source rock from Southern Slope Zone, well M17, 3803 m. Notes: 1 = C_{27} 3-methyltriaromatic steroids; 2 = C_{27} 4-methyltriaromatic steroids; 3 = C_{27} 3-methyltriaromatic steroids + C_{28} 3,24-dimethyltriaromatic steroids; 4 = C_{29} 4,23,24-trimethyltriaromatic steroids; 5 = C_{27} 4-methyltriaromatic steroids + C_{29} 4-methyl-24-ethyltriaromatic steroids; 6 = C_{29} 4,23,24-trimethyltriaromatic steroids; 7 = C_{29} 3-methyl-24-ethyltriaromatic steroids; 8 = C_{29} 4,23,24-trimethyltriaromatic steroids; 9 = C_{29} 4-methyl-24-ethyltriaromatic steroids; 10 = C_{28} 3,24-dimethyltriaromatic steroids; 11 = C_{28} 3,24-dimethyltriaromatic steroids; 12 = C_{29} 4 α ,23,24-trimethyltriaromatic steroids; 13 = C_{29} 4 α ,23,24-trimethyltriaromatic steroids; 14 = C_{29} 3-methyl-24-ethyltriaromatic steroids; 15 = C_{29} 4 α ,23,24-trimethyltriaromatic steroids; 16 = C_{29} 4 α -methyl-24-ethyltriaromatic steroids; 17 = C_{29} 4 α ,23,24-trimethyltriaromatic steroids.

C_{30} 4-Me St and dino-TAS are both derived from dinoflagellates, and the related parameters, such as C_{30} 4-Me/ C_{29} St and TDSI, provide effective means to evaluate the organic matter sources of source rocks and are therefore widely applied for oil–source correlation [37–40]. A negative correlation between C_{30} 4-Me St and dino-TAS can be attributed to the depositional environment, with a sub-oxic and fresh environment being conducive to the formation of C_{30} 4-Me St [41]. All the Els_3 crude oils and source rocks from Southern Slope Zone are closely plotted in Figure 11, indicating strong affinity between them. The Els_3 crude oils from the middle-step area display a close relationship to the Els_3 source rocks of the middle-step area (Figures 8 and 11).

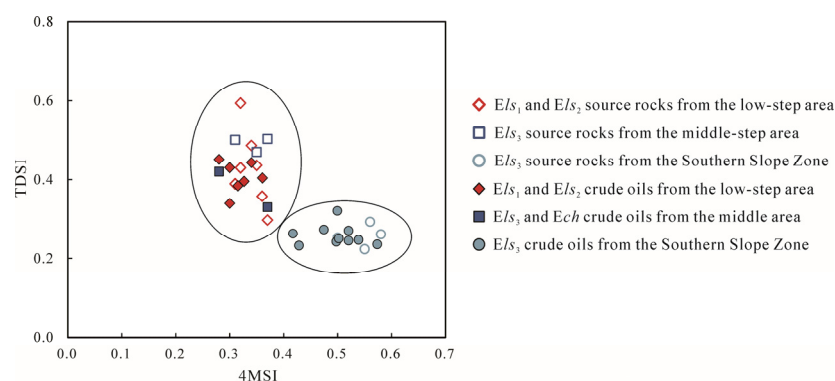


Figure 11. Correlation between the relative abundances of methyl-triaromatic steroids relative abundance in the studied oils and source rocks.

4.2.4. Maturity of Crude Oils

The maturity parameters of aromatic hydrocarbons are widely applied in assessing crude oil maturity [42]. The Phenanthrene Distribution Fraction (MPDF), calculated by the relative abundances of the four isomers of methylphenanthrene, has been used as a thermal maturity indicator [43,44]. According to the cross plot of MPDF parameters (F1 and F2), the crude oils from the low-step area and the Southern Slope Zone are in the mature stage, while the data points of the crude oils from the middle-step area indicate low maturity (Figure 12). The maturity of the crude oils in the middle-step area is the lowest.

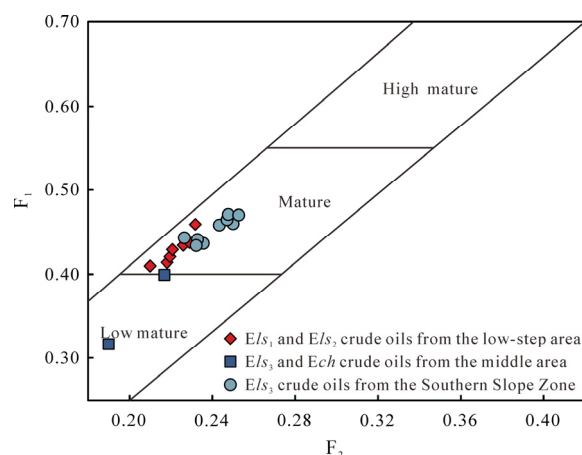


Figure 12. Cross plot of the Methyl-Phenanthrene Distribution Fraction (MPDF) parameters F1 vs. F2 showing the maturity of crude oil samples.

4.3. Modeling of Oil Generation, Migration, and Accumulation

4.3.1. Source Rock Maturity History

The maturity of organic matter is related to the burial depth and heat flow, and vitrinite reflectance (Ro%) is usually applied to evaluate the maturity. The transformation ratio (TR) refers to the proportion of organic matter in the source rock that is transformed into hydrocarbons during the thermal maturation process. Generally, the higher thermal maturity corresponds to the higher TR [45,46]. Figure 13 shows the evolution of the maturity and TR with geological time for the profile AA'.

The Els_2 source rocks in the Huangtong Sag and some of the Els_3 source rocks in the Southern Slope Zone entered the oil generation window ($Ro > 0.5\%$) at 30 Ma. During the period 30–23.5 Ma, the strata were subjected to burial, uplift, and denudation, and the Els_1 source rocks in the Huangtong Sag, some of the Els_2 source rocks in the Southern Slope Zone, and the Els_3 source rocks in the middle step reached the mature stage. The Els_2 source rocks in the Huangtong Sag and the Els_3 source rocks in the Southern Slope Zone apparently entered the main oil generation stage ($Ro > 0.7\%$). At 23.5–10 Ma, since the low deposition rate of Neogene [20], the thermal evolution degree of the source rocks at 10 Ma is similar to that at 23.5 Ma, with a maximum TR exceeding 80%. At present, both the Els_1 and Els_2 source rocks in the Huangtong Sag are in the peak period for oil generation, with maximum Ro up to 1.2% and TR up to 100%. The maximum Ro of the Els_3 source rocks in the middle step is 0.68%, with a TR of 40%.

Comparison of hydrocarbon generation in the different source rocks over geological time indicates that the source rocks in the Fushan Depression began to generate hydrocarbons at 30 Ma (Figure 14). The Els_2 source rocks in the low-step area and the Els_3 source rocks in the Southern Slope Zone are characterized by long hydrocarbon generation periods and large hydrocarbon-generation mass. The Els_3 source rocks in the middle-step area generated hydrocarbons at around 20 Ma, but with the smallest hydrocarbon-generation mass due to their low maturity.

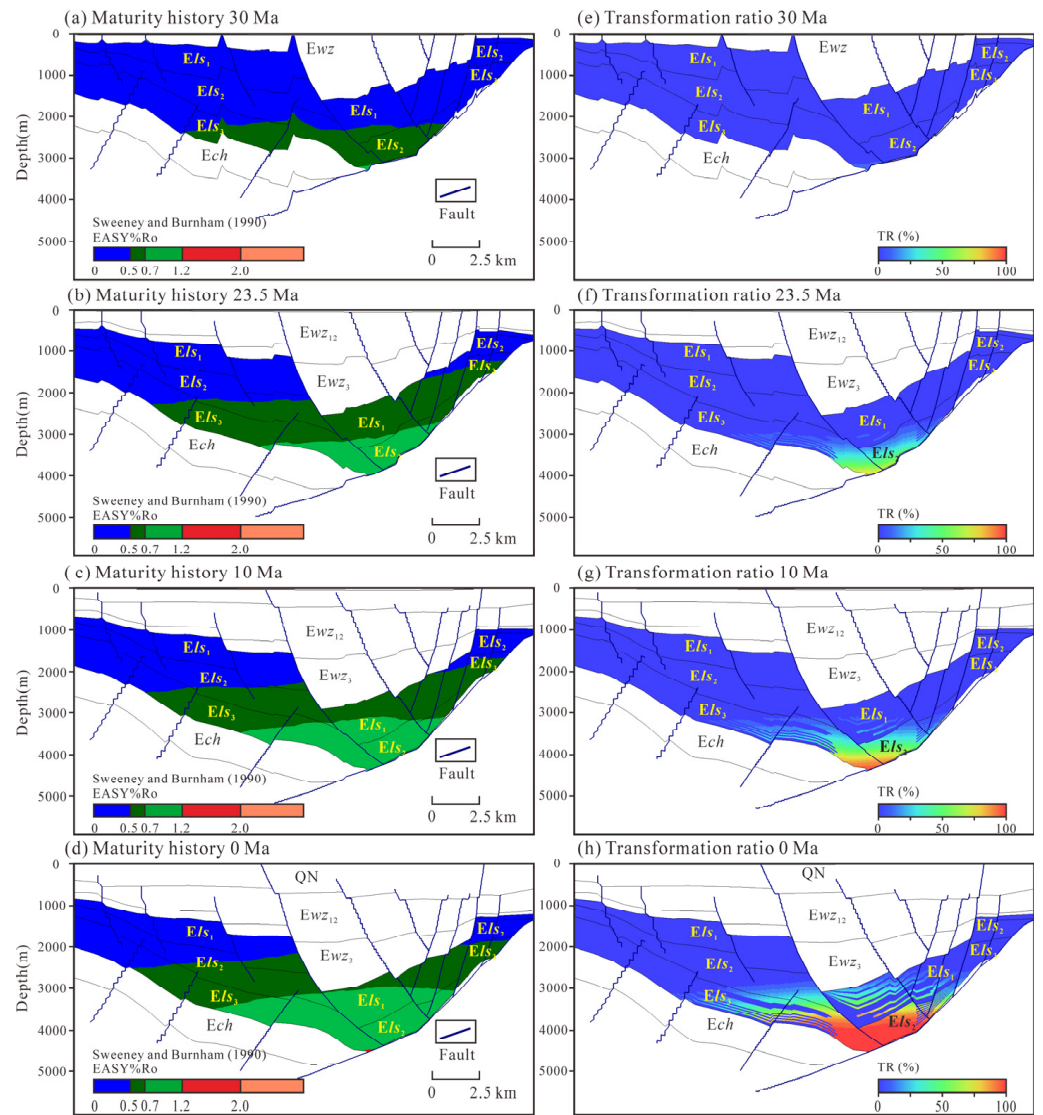


Figure 13. Evolution of the maturity and the transformation ratio with age in Profile AA'. (a) Maturity history at 30 Ma; (b) maturity history at 23.5 Ma; (c) maturity history at 10 Ma; (d) maturity history at 0 Ma; (e) transformation ratio at 30 Ma; (f) transformation ratio at 23.5 Ma; (g) transformation ratio at 10 Ma; (h) transformation ratio at 0 Ma [24].

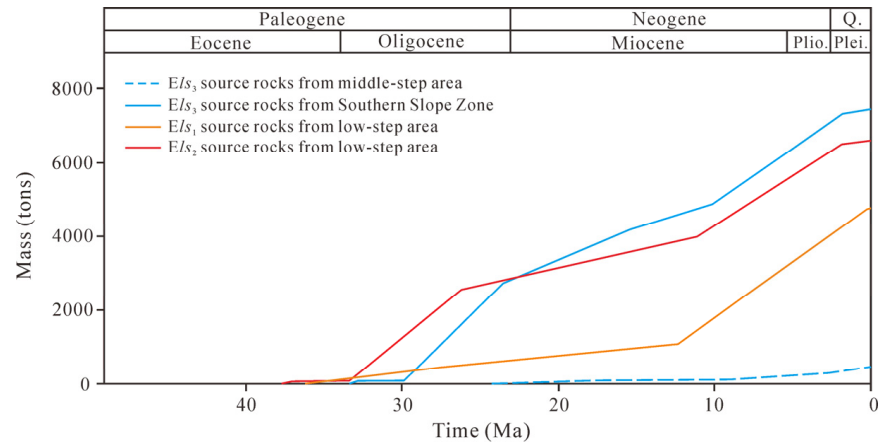


Figure 14. Hydrocarbon generation in different source rocks over geological time.

4.3.2. Hydrocarbon Generation, Migration, and Accumulation History

Figure 15 shows that the simulated oil reservoirs are mostly distributed in the Huangtong Sag and the fault footwall of the Southern Slope Zone, with some hydrocarbon accumulation also occurring in the Els_3 and Ech reservoirs in the middle step. The simulation results are consistent with the actual exploration results of hydrocarbon reservoirs.

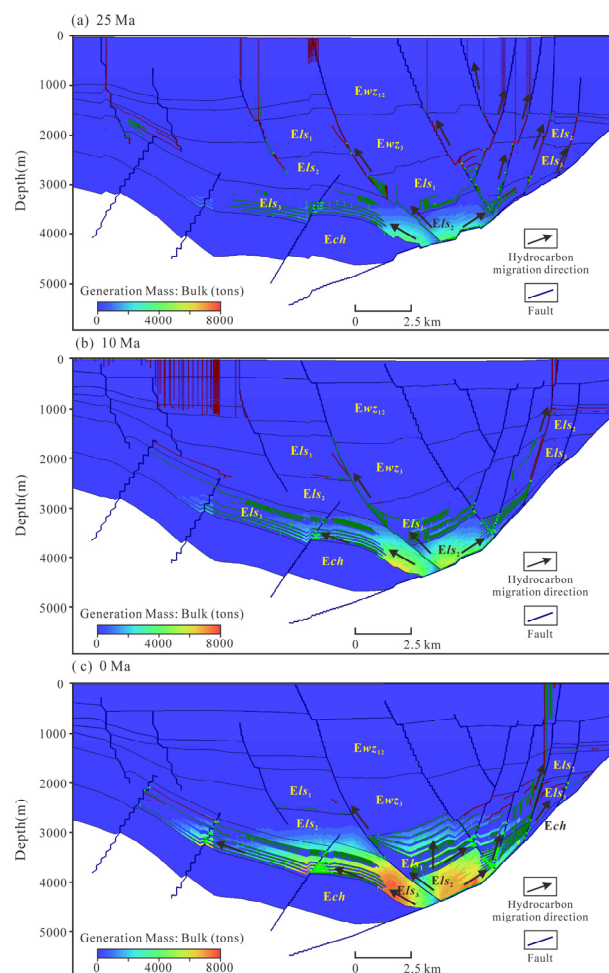


Figure 15. Simulation results of hydrocarbon migration and accumulation in Profile AA'. (a) Hydrocarbon migration and accumulation at 25 Ma; (b) hydrocarbon migration and accumulation at 10 Ma; (c) hydrocarbon migration and accumulation at 0 Ma.

At 25 Ma, most of the hydrocarbons generated from the Els_3 source rocks of the Southern Slope Zone and the Els_2 source rocks of the Huangtong Sag escaped along active faults, particularly the Meihua and Bohou Faults. Due to well sealing of the antithetic faults, only small amounts of hydrocarbons accumulated in the fault footwall of the Southern Slope Zone. At 25–10 Ma, the hydrocarbon generation centers were still concentrated in the Els_3 source rocks of the Southern Slope Zone and the Els_2 source rocks of the Huangtong Sag, with a few accumulations occurring near the hydrocarbon generating center. At 10–0 Ma, the hydrocarbons generated from the Els_3 source rocks migrated along sandbodies to the Southern Slope Zone and accumulated in the fault footwall. The hydrocarbon migration orientation indicated by the geochemical parameters [9] is consistent with the simulation results. The crude oils from the low-step area are mostly distributed in the hanging wall of the consequent fault and the footwall of the antithetic fault. The faults in the low-step area are crucial for hydrocarbon accumulation. The low-step area is adjacent to the hydrocarbon generation center, so the hydrocarbons had to migrate only a short distance along the fault. The hydrocarbons accumulated in the upper part of Els_3 in the middle step area

were generated in the lower part of the Els_3 source rocks, with the consequent fault as the migration conduit. The good sealing properties of the Els_2 thick mudstone in the middle step area, combined with high overburden pressure, caused the hydrocarbons to migrate downwards along the fault to the Changliu Reservoir.

4.3.3. Fluid Inclusion Evidence

Two oil sands from Ech in well Ch23 were sampled for homogenization temperature measurement of their fluid inclusions. The sandstone samples exhibited pale yellow fluorescence, and their homogenization temperatures ranged from 90 to 95 °C. The depositional burial and thermal histories of well Ch23 were reconstructed using Petromod-1D software, calibrated according to the measured Ro . The maximum current buried temperature is 98° (Figure 16). The episodes and timing of oil charging were determined from the reconstructed burial and thermal histories, indicating that the main oil charging time in the Ech reservoirs in Well Ch23 was from the end of the mid-Miocene to the early Pliocene (8–3 Ma), with only a single charging episode occurring. The oil charging time of the Southern Slope Zone and the low-step area was determined to be between 10 and 0 Ma [9,11].

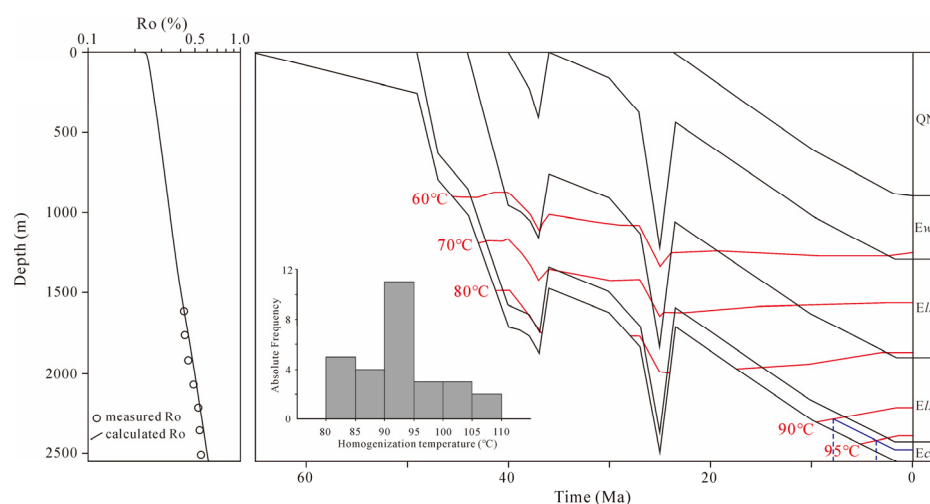


Figure 16. Timing and episodes of oil charging based on fluid inclusion observation and burial history—thermal history reconstruction of the Well Ch23.

4.4. Implications for Petroleum Exploration

Based on the systematic oil-oil and oil-source rock correlations, the crude oils in this study can be divided into three types, two of which have been reported in previous studies [9,10]. The oil migration and accumulation model for the study area is shown in the Figure 17. In terms of the static factors and dynamic processes for hydrocarbon accumulation, three petroleum system—the Southern Slope Zone petroleum system, the Huangtong Sag petroleum system and the Chaoyang middle-step petroleum system—are divided by the Meihua Fault and Bohou Fault.

The crude oils in the Els_3 reservoir in the Southern Slope Zone were generated from the Els_3 source rocks. The hydrocarbons migrated southward along the sandbodies and accumulated in the footwall of the antithetic fault. The hydrocarbon in the Huangtong Sag petroleum system migrated upwards along the fault, which is verified by the parameters of geochemical tracers, such as 4-/1-methylidibenzothiophene and 1-/4-methylidibenzofuran [9]. The Els_3 and Ech oils from the middle step area—of a previously unreported type—were generated from the Els_3 source rocks in the middle step area.

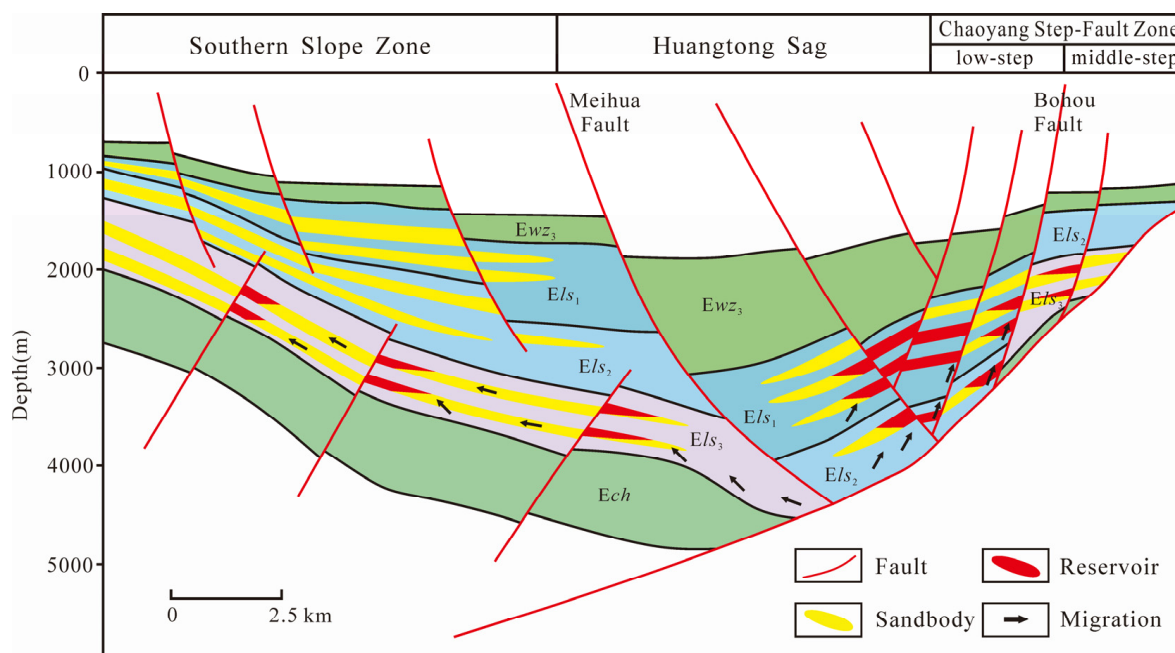


Figure 17. A conceptual model showing oil migration and accumulation in the Chaoyang Step-Fault Zone.

Although the Els_3 source rocks in the middle step area are thought to be good to excellent source rocks, their poor hydrocarbon generation capacity in situ is revealed by the two-dimensional simulation and can be explained by their shallow burial depth. Despite the discovery of these new-type oils in the middle-step area, hydrocarbon shows have only occurred in a few wells. The low-step area is a more favorable exploration area than the middle-step area because of its near-source advantages.

5. Conclusions

The crude oils from the middle-step area are identified for the first time as a new oil group. This new oil group was generated locally from the Els_3 source rocks in the middle-step area. The principal distinguishing factors between the two established oil groups and this new group are the distributions of $C_{19}\sim C_{23}$ tricyclic terpanes, oleanane, C_{30} 4-methyl-24-ethylcholestanes, and methyl triaromatic dinosteroids.

Three petroleum systems—the Southern Slope Zone petroleum system, the Huangtong Sag and low-step petroleum system, and the Chaoyang middle-step petroleum system—are divided by the Meihua Fault and Bohou Fault. The hydrocarbons generated from the Els_1 and Els_2 source rocks in the Huangtong Sag migrated to the Els_1 and Els_2 reservoirs in the lower-step area. The source rocks in the Huangtong Sag are in the peak oil generation stage at present, while the Els_3 source rocks in the middle-step area are in the early stage, with the hydrocarbons migrating along the fault to the upper part of the Els_3 reservoir. Only one hydrocarbon charging episode has been identified for the middle-step area, around the end of the middle Miocene to the early Pliocene (10–0 Ma).

Although the hydrocarbon shows have occurred in the Els_3 and Ech in the middle-step area, the resource potential of the middle-step area is limited by its shallow burial depth. The low-step area, adjacent to the Huangtong Sag, is a more favorable exploration area due to its proximity to its source. The footwall of the antithetic fault near the Huangtong Sag is identified as the most favorable exploration target.

Author Contributions: Conceptualization, Y.S. and H.G.; methodology, X.L. and H.L.; software, X.L. and X.W.; validation, M.L., S.D. and X.H.; formal analysis, M.L., S.D. and X.H.; investigation, M.L., S.D. and X.H.; resources, X.W.; data curation, X.W.; writing—original draft preparation, Y.S.; writing—review and editing, H.G. and X.L.; visualization, H.G.; supervision, Y.S., S.D. and X.H.;

project administration, H.L.; funding acquisition, Y.S and H.L. All authors have read and agreed to the published version of the manuscript.

Funding: This study was funded by the South Oil Exploration and Development Company of PetroChina (2024-HNYJ-018).

Data Availability Statement: The original contributions presented in the study are included in the article, further inquiries can be directed to the corresponding author.

Acknowledgments: The authors would like to thank Shi Shengbao, Zhu Lei, and Zhang Jianfeng of China University of Petroleum (Beijing) for their assistance and guidance during the experiment. We also appreciate the reviewers and editors for their suggestions and comments.

Conflicts of Interest: Authors Yang Shi, Hao Guo, Xiaohan Li and Huiqi Li were employed by the Southern Oil Exploration and Development Company. The remaining authors declare that the research was conducted in the absence of any commercial or financial relationships that could be construed as a potential conflict of interest.

References

- Schwangler, M.; Harris, N.B.; Waldron, J.W.F. Source rock characterization and oil-to-source rock correlation of a Cambrian-Ordovician fold-and-thrust belt petroleum system, western Newfoundland. *Mar. Petrol. Geol.* **2020**, *115*, 104283. [\[CrossRef\]](#)
- Hu, L.G.; Fuhrmann, A.; Poelchau, H.S.; Horsfield, B.; Zhang, Z.W.; Wu, T.S.; Chen, Y.X.; Li, J.Y. Numerical simulation of petroleum generation and migration in the Qingshui sag, western depression of the Liaohe basin, northeast China. *AAPG Bull.* **2005**, *89*, 1629–1649. [\[CrossRef\]](#)
- Shabani, F.; Amini, A.; Tavakoli, V.; Honarmand, J.; Gong, C.R. 3D forward stratigraphic modeling of the Albian succession in a part of the northeastern margin of the Arabian Plate and its implications for exploration of subtle traps. *Mar. Petrol. Geol.* **2022**, *145*, 105880. [\[CrossRef\]](#)
- Zeng, B.; Li, M.J.; Wang, X.; Wang, F.Z.; Gong, C.L.; Lai, J.; Shi, Y. Source rock evaluation within a sequence stratigraphic framework of the Paleogene Liushagang Formation in the Fushan Depression, South China Sea. *Geol. J.* **2022**, *57*, 2409–2427. [\[CrossRef\]](#)
- Zeng, B.; Li, M.J.; Wang, N.; Shi, Y.; Wang, F.Z.; Wang, X. Geochemistry and heterogeneous accumulation of organic matter in lacustrine basins: A case study of the Eocene Liushagang Formation in the Fushan Depression, South China Sea. *Petrol. Sci.* **2022**, *19*, 2533–2548. [\[CrossRef\]](#)
- Liu, E.T.; Wang, H.; Lin, Z.L.; Li, Y.; Ma, Q.L. Characteristics and hydrocarbon enrichment rules of transfer zone in Fushan Sag, Beibuwan Basin. *J. Cent. South Univ. Sci. Technol.* **2012**, *43*, 3946–3953. (In Chinese)
- Liu, E.T.; Wang, H.; Li, Y.; Leonard, N.D.; Feng, Y.X.; Pan, S.Q.; Xia, C.Y. Relative role of accommodation zones in controlling stratal architectural variability and facies distribution: Insights from the Fushan Depression, South China Sea. *Mar. Pet. Geol.* **2015**, *68*, 219–239. [\[CrossRef\]](#)
- Zhang, Z.W.; Liu, Z.F.; Zhang, G.C.; Zhao, Z.G.; Xu, J.Y. The chasmic stage and structural evolution features of Beibuwan Basin. *J. Oil Gas Technol.* **2013**, *35*, 6–10.
- Li, M.J.; Wang, T.G.; Liu, J.; Zhang, M.Z.; Lu, H.; Ma, Q.L.; Gao, L.H. Oil charging orientation and accumulation characteristics of oil reservoirs in the Fushan sag, Beibuwan basin. *Pet. Geol. Exp.* **2007**, *29*, 172–177. (In Chinese)
- Gan, H.J.; Wang, H.; Shi, Y.; Ma, Q.L.; Liu, E.T.; Yan, D.T.; Pan, Z.J. Geochemical characteristics and genetic origin of crude oil in the Fushan sag, Beibuwan Basin, South China Sea. *Mar. Pet. Geol.* **2020**, *112*, 104114. [\[CrossRef\]](#)
- Gan, H.J.; Gong, S.; Tian, H.; Wang, H.; Chen, J.; Ma, Q.L.; Liu, K.X.; Lv, Z.H. Geochemical characteristics of inclusion oils and charge history in the Fushan Sag, Beibuwan Basin, South China Sea. *Appl. Geochem.* **2023**, *150*, 105598. [\[CrossRef\]](#)
- Wang, G.H.; Wang, H.; Gan, H.J.; Shi, Y.; Zhao, Y.D.; Chen, S.B. Oil source and migration process in oblique transfer zone of Fushan Sag, northern South China Sea. *J. Cent. South Univ.* **2016**, *23*, 654–668. [\[CrossRef\]](#)
- Qi, Z.G.; Lu, Z.H.; Jiang, F.J.; Song, Z.Z.; Chen, D.; Zhang, Y.Q.; Guo, J.; Fang, Z.; Wang, X.R.; Liu, Y.L. Controlling factors of hydrocarbon distribution and source-migration-accumulation model in Fushan Depression. *J. China Univ. Min. Technol. Chin. Ed.* **2024**, *53*, 777–792. (In Chinese)
- Wang, X.; Lu, Z.H.; Li, M.J.; Guo, H.; Zhu, Z.L.; Li, X.H.; Yang, C.Y.; Zeng, B.; Wang, F.Z.; Ran, Z.C. Petroleum charging history of the Paleogene sandstone reservoirs in the Huangtong Sag of the Fushan Depression, South China Sea. *Energies* **2022**, *15*, 1374. [\[CrossRef\]](#)
- Lu, Z.H.; Gan, H.J.; Shi, Y.; Chen, S.B.; Wang, H.; Ma, Q.L. Geochemical Characteristics of crude oil and oil-source correlation in the western Fushan Depression. *Earth Sci.* **2016**, *41*, 1909–1920. (In Chinese)
- Li, M.J.; Wang, T.G.; Liu, J.; Zhang, M.Z.; Lu, H.; Ma, Q.L.; Gao, L.H. Characteristics of oil and gas accumulation in Yong'an-Meitai area of the Fushan Depression, Beibuwan Basin, South China Sea. *Pet. Sci.* **2007**, *4*, 23–33.
- Qin, Q.H.; Lei, D.; Song, X.W.; Su, J.Q.; Ren, G.Y.; Liu, D.S.; Ma, Q.L.; Lu, Z.H.; Guo, H.; Liao, F.Y.; et al. Geological conditions and the main controlling factors for the tight oil accumulation in Liushagang Formation of Fushan Depression, Beibuwan Basin. *Bull. Geol. Sci. Technol.* **2021**, *40*, 1–10. (In Chinese)

18. Ma, Q.L.; Zhao, S.E.; Liao, Y.T.; Lin, Z.L. Sequence architectures of Paleogene Liushagang Formation and its significance in Fushan Sag of the Beibuwan Basin. *J. China Univ. Geosci. Chin. Ed.* **2012**, *37*, 667–678. (In Chinese)
19. Liu, E.T.; Wang, H.; Li, Y.; Zhou, W.; Leonard, N.D.; Lin, Z.L.; Ma, Q.L. Sedimentary characteristics and tectonic setting of sublacustrine fans in a half-graben rift depression, Beibuwan Basin, South China Sea. *Mar. Pet. Geol.* **2014**, *52*, 9–21. [[CrossRef](#)]
20. Song, Q.Q.; Hu, J.; Lei, D.; Li, Z.W.; Tang, R.; Hu, S.B. Provenance evolution of the Fushan Sag (Hainan Island, Southern China): Constraints from U-Pb geochronology on detrital zircons. *Mar. Pet. Geol.* **2024**, *168*, 107037. [[CrossRef](#)]
21. Li, Y.; Lin, S.; Wang, H.; Luo, D. Depositional setting analysis using seismic sedimentology: Example from the Paleogene Liushagang sequence in the Fushan depression, South China Sea. *Geodesy Geodyn.* **2017**, *8*, 347–355. [[CrossRef](#)]
22. Al-Hajeri, M.M.; Al Saeed, M.; Derks, J.; Fuchs, T.; Hantschel, T.; Kauerauf, A.; Neumaier, M.; Schenk, O.; Swientek, O.; Tessen, N. Basin and petroleum system modeling. *Oilfield Rev.* **2009**, *21*, 14–29.
23. Burnham, A.K.; Sweeney, J.J. A chemical kinetic model of vitrinite maturation and reflectance. *Geochim. Cosmochim. Acta* **1989**, *53*, 2649–2657. [[CrossRef](#)]
24. Sweeney, J.J.; Burnham, A.K. Evaluation of a simple model of vitrinite reflectance based on chemical kinetics. *AAPG Bull.* **1990**, *74*, 1559–1570.
25. Chen, L.; Gan, H.; Zhu, C.; Tian, J. Study on Subsidence History of Weixinan Sag, Beibuwan Basin. *J. Xinjiang Pet. Inst.* **2002**, *14*, 12–17. (In Chinese)
26. Chen, S.B.; Gan, H.J.; Xia, C.Y.; Zhao, Y.D.; Wang, G.H.; Wang, X. History simulation of thermal evolution and hydrocarbon generation of source rocks in Bailian sub-Sag, Fushan Sag, Beibuwan Basin. *Xinjiang Pet. Geol.* **2014**, *35*, 672–677. (In Chinese)
27. Zeng, B.; Lu, Z.; Yang, T.; Shi, Y.; Guo, H.; Wang, X.; Liao, F.; Li, M. Hydrocarbon Generation History of the Eocene Source Rocks in the Fushan Depression, South China Sea: Insights from a Basin Modeling Study. *Processes* **2023**, *11*, 2051. [[CrossRef](#)]
28. Wygrala, B.P. *Integrated Study of an Oil Field in the Southern Po Basin, Northern Italy*; KFK: Karlsruhe, Germany, 1989; 325p.
29. Robison, C.R.; Smith, M.A.; Royle, R.A. Organic facies in Cretaceous and Jurassic hydrocarbon source rocks, Southern Indus basin, Pakistan. *Int. J. Coal Geol.* **1999**, *39*, 205–225. [[CrossRef](#)]
30. Mukhopadhyay, P.K.; Wade, J.A.; Kruge, M.A. Organic facies and maturation of Jurassic/Cretaceous rocks, and possible oil-source rock correlation based on pyrolysis of asphaltene, Scotian Basin, Canada. *Org. Geochem.* **1995**, *22*, 85–104. [[CrossRef](#)]
31. Xiao, H.; Li, M.J.; Yang, Z.; Zhu, Z.L. The distribution patterns and geochemical implication of C19–C23 tricyclic terpanes in source rocks and crude oils occurred in various depositional environment. *Geochemica* **2019**, *48*, 161–170. (In Chinese)
32. Xiao, H.; Li, M.J.; Nettersheim, B.J. Short chain tricyclic terpanes as organic proxies for paleo-depositional conditions. *Chem. Geol.* **2024**, *652*, 122023. [[CrossRef](#)]
33. Samuel, O.J.; Kildahl-Andersen, G.; Nytoft, H.P.; Johansen, J.E.; Jones, M. Novel tricyclic and tetracyclic terpanes in Tertiary deltaic oils: Structural identification, origin and application to petroleum correlation. *Org. Geochem.* **2010**, *41*, 1326–1337. [[CrossRef](#)]
34. Xiao, H.; Wang, T.G.; Li, M.J.; Fu, J.; Tang, Y.J.; Shi, S.B.; Yang, Z.; Lu, X.L. Occurrence and Distribution of Unusual Tri- and Tetracyclic Terpanes and Their Geochemical Significance in Some Paleogene Oils from China. *Energy Fuels* **2018**, *32*, 7393–7403. [[CrossRef](#)]
35. Peters, K.E.; Moldowan, J.M. *The Biomarker Guide: Interpreting Molecular Fossils in Petroleum and Ancient Sediments*, 2nd ed.; Cambridge University Press: Cambridge, UK, 2005; pp. 572–575.
36. Fu, J.; Chen, C.; Li, M.J.; Zhang, Z.T.; Long, Z.L.; Wang, T.G.; Lu, X.L. Petroleum charging history of Neogene reservoir in the Baiyun Sag, Pearl River Mouth Basin, South China sea. *J. Pet. Sci. Eng.* **2020**, *190*, 106945. [[CrossRef](#)]
37. Xiao, H.; Li, M.J.; Liu, J.G.; Mao, F.J.; Cheng, D.S.; Yang, Z. Oil-oil and oil-source rock correlations in the Muglad Basin, Sudan and South Sudan: New insights from molecular markers analyses. *Mar. Petrol. Geol.* **2019**, *103*, 351–365. [[CrossRef](#)]
38. Boon, J.J.; Rijpstra, W.I.C.; De Lange, F.; De Leeuw, J.W.; Yoshioka, M.; Shimizu, Y. Black sea sterol-a molecular fossil for dinoflagellate blooms. *Nature* **1979**, *277*, 125–127. [[CrossRef](#)]
39. You, B.; Ni, Z.Y.; Chen, J.F.; Wang, G.L.; Xiao, H.; Wang, Y.S.; Song, G.Q. A distinct oil group in the Dongying Depression, Bohai Bay Basin, China: New insights from norcholestane and triaromatic steroid analyses. *Org. Geochem.* **2021**, *162*, 104316. [[CrossRef](#)]
40. Wang, D.Y.; Li, M.J.; Yang, L.; Yang, Y.F.; Li, E.T.; Jin, J.; Zou, X.L.; Xu, B.D. The distribution of triaromatic steroids in Permian source rocks and implications for oil-source correlations in the Mahu Sag, Junggar Basin, NW China. *Nat. Gas Geosci.* **2022**, *33*, 1862–1873. (In Chinese)
41. Chang, R.; Wang, G.L.; Zhang, Z.H.; Li, H.Y.; Cao, L.; Xia, H.Y. Distribution and Genesis of Dinoflagellate-derived Molecular Fossils in Beibuwan Basin. *Acta Sedimentol. Sin.* **2023**, *41*, 280–288. (In Chinese)
42. Chakhmakhchev, A.; Suzuki, N. Saturate biomarkers and aromatic sulfur compounds in oils and condensates from different source rock lithologies of Kazakhstan, Japan and Russia. *Org. Geochem.* **1995**, *23*, 289–299. [[CrossRef](#)]
43. Kvalheim, O.M.; Christy, A.A.; Telnaes, N.; Bjørseth, A. Maturity determination of organic matter in coals using the methylphenanthrene distribution. *Geochim. Cosmochim. Acta* **1987**, *51*, 1883–1888. [[CrossRef](#)]
44. Bao, J.P.; Wang, T.G.; Zhou, Y.Q.; Yu, F.X.; Wang, J.J.; Zhou, Q.L.; Chen, F.J. The relationship between methyl phenanthrene ratios and the evolution of organic matter. *J. Jiangnan Pet. Inst.* **1992**, *14*, 8–19. (In Chinese)

45. Makeen, Y.M.; Abdullah, W.H.; Pearson, M.J.; Hakimi, M.H.; Ayinla, H.A.; Elhassan, O.M.; Abas, A.M. History of hydrocarbon generation, migration and accumulation in the Fula sub-basin, Muglad Basin, Sudan: Implications of a 2D basin modeling study. *Mar. Pet. Geol.* **2016**, *77*, 931–941. [[CrossRef](#)]
46. Yang, S.B.; Li, M.J.; Wang, Y.S.; Xiao, H.; Huang, S.Q.; Kang, W.J.; Wang, F.Z. Origin, Migration, and Characterization of Gas in the Xinglongtai Area, Liaohu Subbasin (Northeast China): Insight from Geochemical Evidence and Basin Modeling. *Energies* **2023**, *16*, 6429. [[CrossRef](#)]

Disclaimer/Publisher’s Note: The statements, opinions and data contained in all publications are solely those of the individual author(s) and contributor(s) and not of MDPI and/or the editor(s). MDPI and/or the editor(s) disclaim responsibility for any injury to people or property resulting from any ideas, methods, instructions or products referred to in the content.